Research Article

Waad Adnan Khalaf* and Mohsin Noori Hamzah

Experimental and numerical studies of ballistic resistance of hybrid sandwich composite body armor

https://doi.org/10.1515/eng-2022-0543 received September 03, 2023; accepted October 16, 2023

Abstract: Defense mechanisms remain important and indispensable due to the different types of pistols and ordnance besides many guns. Hybrid composite sandwich panels are an attractive focus because of their ingrained characteristics, such as high stuffiness and high energy absorption. Hybrid composite sandwich panels are among the most important in armoring various structures. Despite the high density of these panels, they have significant qualities that qualify them to be the first selection for use in armored vehicles or body armor. Recently, there have been several types of structures, and selecting the appropriate structure as armor against the projectiles is very important. The study subjected three samples to the ballistic impact test using a 7.62 × 39 mm bullet. The first sample, S1, consists of ultra high molecular weight polyethylene (UHMWPE)/epoxy, unfilled honeycomb core, Kevlar/epoxy, unfilled honeycomb core, Kevlar/epoxy, and UHMWPE/epoxy; the second sample, S2, comprises Kevlar/epoxy, unfilled honeycomb core, Kevlar/ epoxy, unfilled honeycomb core, and UHMWPE/epoxy, and the third sample, S3, comprises Al₂O₃, Kevlar/epoxy, unfilled honeycomb core, carbon/epoxy, unfilled honeycomb core, and carbon/epoxy. ABAQUS software was used to evaluate the ballistic impact numerically, and after that, the study examined the same armor samples experimentally. The results manifested that only the armor S3 succeeded in stopping the bullet. This is attributed to the structure of the cores, which helps compress and accumulate the cells under the projectile. The speeds of the bullet after penetration (residual velocity; VR) were 748.5 and 715.3 m/s for S1 and S2 armors, respectively, where the back face signature for S3 was 1.5 mm, which

is optimum and within the allowed range. The total energy absorption of these armors S1, S2, and S3 is 344.65, 539.04, and 2585.66 J. Furthermore, the highest deviation between numerical and experimental approaches is about 2.04% in the VR.

Keywords: ballistic impact, 7.62 × 39 mm bullet, hybrid sandwich armor, energy absorption, back face signature

1 Introduction

One of the primary issues for engineers and researchers in ballistic armor against bullets and shrapnel is the requirement for high-level ballistics for military and defense sectors. In recent years, terrorist attacks and wars have increased. This is because donning body armor has prevented armies and warriors from losing countless lives while waging wars and conducting counterterrorism operations. According to the research conducted during the Iraq warfare in 2003, 58% of the wounds were medium, while 9% were in the eyes, legs, or hands, and several of the wounds infected the trunk [1].

Furthermore, body armor is spaciously employed in peacekeeping and public security missions. According to statistics, ballistic-resistant body armor supplied by international police enforcement forces has recently kept over 3,000 cops on the beat. Personnel armor is designed to withstand bullets, fragments, and small 2-caliber projectiles [2]. The degree to which a person is protected from a ballistic attack provided by these armaments is determined by the kinetic energy that bullets deliver, which can be sealed with the armor. The National Institute of Justice (NIJ) has issued a report detailing defamatory threats. The whole plane of safeguard and bomb gender has its requirements [3]. Several armor solutions for effective ballistic protection use advanced alloys, ceramics, and composite materials. One of these important solutions is the sandwich structure together with composite materials [4].

The concepts of science underlying the construction of sandwich armor structures must be understood to satisfy

^{*} Corresponding author: Waad Adnan Khalaf, Mechanical
Engineering Department, University of Technology-Iraq, Alsina'a Street,
10066, Baghdad, Iraq, e-mail: me.19.35@grad.uotechnology.edu.iq
Mohsin Noori Hamzah: Mechanical Engineering Department, University
of Technology-Iraq, Alsina'a Street, 10066, Baghdad, Iraq,
e-mail: mohsin.n.hamzah@uotechnology.edu.iq

the armor industry's demands better. The industry still needs to overcome significant hurdles, such as mobility and protection, despite the enormous effort to grasp these concepts, particularly concerning armor textiles and composite. Mobility and protection are the two main requirements of the users of armor materials. The lightest armor materials are required for ballistic armors to improve mobility. On the other hand, defensive qualities improve as the armor material weight increases, which restricts movement. Research into armor materials now primarily focuses on weight reduction and strength development to improve mobility and conserve user energy. As a result, the field was attracted to a lightweight, flexible, and highly energy-absorbent material. Sandwich composites changed the game thanks to their high-rigidity and lightweight structure. Composite materials that enable large-scale manufacture are gaining interest due to various reinforcing elements' availability and novel processing techniques' development [5]. Numerous studies are now looking into ways to enhance the performance of composite structures. To enhance the energy-absorbing qualities of the structures without losing sight of the overall weight, researchers are examining alternative settings for sandwich composite materials. Other parameters that can be changed to enhance the performance of sandwich composite structures include material qualities, thickness, and core characteristics. The ballistic armor performance has been improved thanks to the use of cuttingedge materials in producing armor systems [6].

Several studies have examined the ballistic resistance of sandwich structures and hybrid composites to understand the characteristics of the materials and their effectiveness when subjected to impact loads. Stanislawek et al. [7] modeled a pyramidal ceramic (Al₂O₃) in the front face of armor with a ductile aluminum alloy (AA2024) in the back face besides different arrangements of ceramic structure and AA2024 in other models, and this structure was impacted by armor piercing (AP) projectiles. The experimental and numerical studies proved that pyramidal ceramic armor could resist a projectile threat due to the change in its trajectory [7]. Liu et al. (2016) simulated the fish skin to produce a protection system collected between effective resistances to external loads with superior flexibility. The scales comprise silicon carbide ceramic and aluminum (Al6061-T6) materials in the outer and inner faces, respectively. FEM has been used to simulate the ballistic impact of steel bullets on the scaled armor. The numerical results displayed that the depth of penetration (DOP) and the residual velocity (VR) of the scales decreased with the increase in the thickness of composite scales; furthermore, the inclination of the scale led to eroding and a slip of the projectile, and this is very important to absorb the kinetic energy of the projectile [8].

Mullaoğlu et al. investigated how polycarbonate (PC) projectile dynamically impacts at varied speeds. The numerical test of a PC plate under impact was examined using LS-DYNA. The findings demonstrated that the PC materials are significantly more impact-resistant than other materials [9]. Hu et al. used three types of a mosaic of silicon carbide (SiC) with a ultra high molecular weight polyethylene (UHMWPE) plate to resist the impact of an AP bullet. The geometry of mosaic was square, cylindrical, and hexagonal in the front face. The test results offered a significant enhancement in the ballistic resistance of armor and proved the effect of geometry on the ballistic performance of the armor [10]. Oliveira Braga et al. evaluated the multilayered armor system that was impacted by a projectile; the front face of the system consists of the hexagonal convex or flat ceramic tile, and the aramid fabric and aluminum plate arrangement are in the middle and last layer, respectively. The test presents satisfactory results regarding the back face signature (BFS) and the superior performance of convex ceramic tile [11].

Liu et al. exhibited the high-strength material (UHMWPE) with a high-energy absorption material and structure (EAMS) to construct a new type of armor. The hybrid panel was used against the high speed of spherical bullets. The UHMWPE was used in the front of the panel, and the hollow cylinders of EAMS were utilized in the back. The experimental and numerical results of the study exhibited an increase in the ballistic performance of the panel compared with the pure UHMWPE [12]. Eventually, Yang et al. [13] designed sandwich panels made from the carbon fiber composite in the front face, then the aluminum alloy and the core of this structure made from the pyramidal truss. For these sandwich panels, an experimental and numerical test was done to evaluate this structure, and the result elucidated the considerable amount of energy absorption [13]. According to the literature reviews above, research was conducted on how well the sandwich structures can survive the bullets.

It was also concluded that the various sandwich structure reviews are mostly directed at the test of metallic sandwich structures. Only a few works have been carried out using composite sandwich structures that consist of metallic honeycomb core and composite skins. This study presented a hybrid sandwich structure with an aluminum honeycomb as the core, ceramic tiles, steel plates, and Kevlar fibers reinforced polymers as the skins. Finally, the hybrid sandwich panels were fabricated from Kevlar fibers, SiC ceramic tiles, steel plate, and aluminum honeycomb in this work. Two hybrid sandwich specimens were fabricated utilizing the hand lay-up method for sheets and the water jet machine cutting for the aluminum honeycomb core.

2 Experimental work

2.1 Materials used

The first step in the experimental work is to choose the right materials. The materials used in the manufacturing process for the present work are listed below and shown in Figure 1.

- 1. Aluminum honeycomb
- 2. Aluminum oxide tiles (Al₂O₃)
- 3. Composite material (UHMWPE, Kevlar and carbon fibers, and epoxy resin)
- 4. MS hybrid polymer silicon

The aluminum honeycomb was purchased from "Huarui Honeycomb Technology Co., Ltd, China." The aluminum oxide ceramic tiles (Al₂O₃) were bought from "Ningxia Northern Hi-Tech Industry Co., Ltd., China." The woven Kevlar, woven carbon and unidirectional UHMWPE fibers were purchased from "Wuxi GDE Technology Co., Ltd. China." Epoxy resin type (Sikadur 52LB) was purchased from Sikadur Company. MS hybrid polymer silicon was bought from SOUDAL Company. Mechanical properties of Kevlar, carbon and UHMWPE fibers, and epoxy [14], aluminum alloy (AL3003) [15] and aluminum oxide ceramic are defined in previous literature [16].

2.2 Composite fabrication process

The composite material was prepared using the hand layup technique, which is the open molding technique to fabricate the composite materials. This study used this method to fabricate high-performance composites consisting of a matrix material (epoxy) reinforced by the layers of Kevlar, carbon, and UHMWPE fibers. After that, the mold (glass sheet) was prepared for brushing by covering the inner surface via a layer of wax to guarantee no adhesion between the woven fabric and the mold to facilitate the laminate removal. Then, the base material of epoxy was manually mixed with the hardener, taking into account that the weight percent between hardener and epoxy is 3:1. At room temperature, the fabric was manually placed in the mold and then the resin matrix was brushed on the laminates of reinforcing material until it covered all the layers. Another glass sheet was laid on top of the laminated fibers, and the excess resin was allowed to escape from the sides. An appropriate load was used to press the fiber and epoxy mixture. Finally, after completing the hand lay-up process, the sample was left for 24 h at room temperature before opening the mold. Figure 2 shows the mold and fabrication process, and Figure 3 depicts the final shape of the composite.

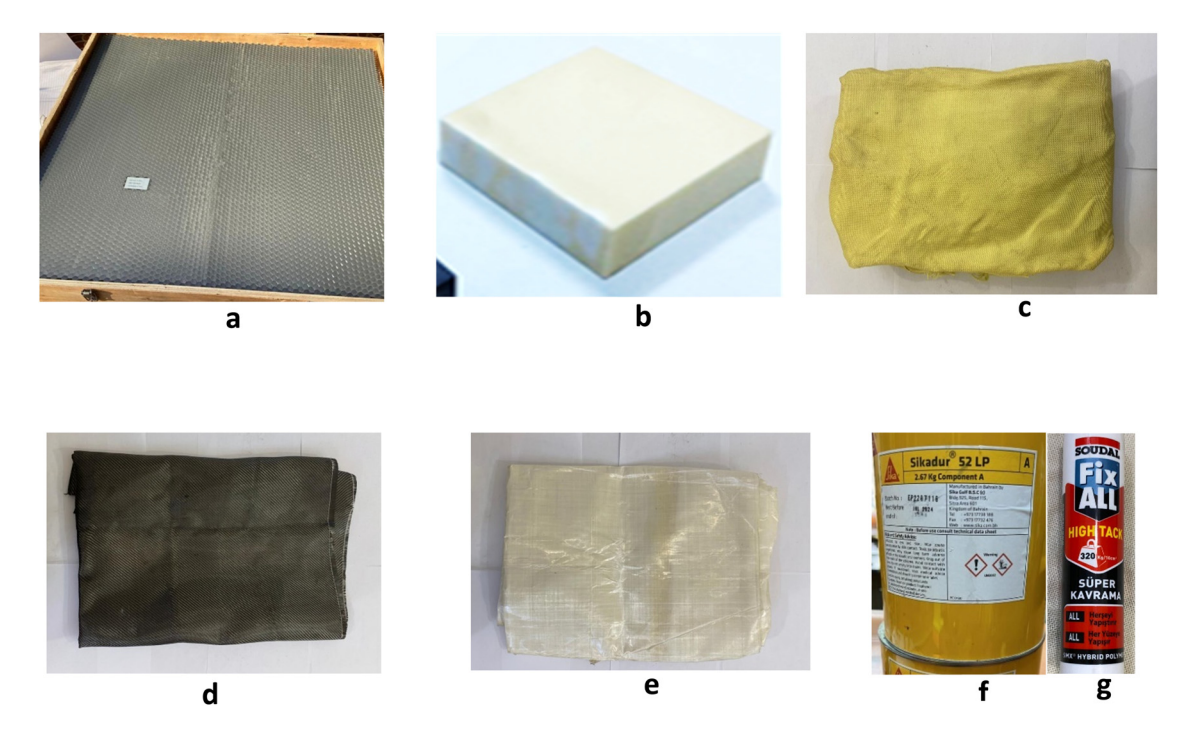


Figure 1: The main materials used in the armor. (a) aluminum honeycomb, (b) aluminum oxide (Al₂O₃) tiles, (c) Kevlar fibers, (d) carbon fibers, (e) UHMWPE fibers, (f) epoxy resin, and (g) MS hybrid polymer silicon.



Figure 2: The mold and the fabrication process.

2.3 Preparation of aluminum honeycomb

Using a water jet cutter machine, the aluminum honeycomb structure was cut to the required dimension (150 \times 150 mm). This machine works depending on the principle of micro erosion, which occurs due to the large volume of the water jet through a very small-diameter bore of the nozzle (0.2–0.3 mm) with a very high jet speed, about

869 m/s with huge kinetic energy. Figure 4 reveals the photo of this machine with the nozzle. The water jet cutting machine owns main sub-systems, such as the water and abrasive tank, a high-pressure pump used to compress water up to 3,000 bar to generate sufficient kinetic energy for cutting, high-pressure valves, and a hydraulic unit. Figure 5 illustrates the final shape of aluminum honeycomb after cutting. To control the cutting process, this

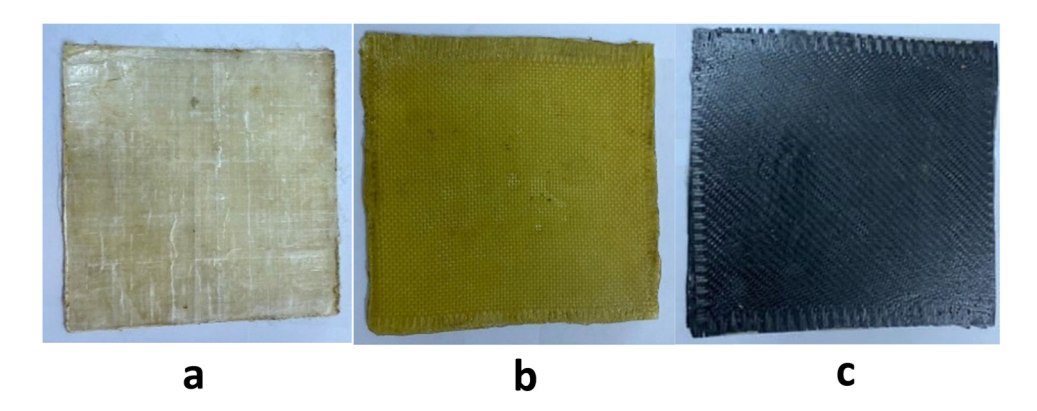


Figure 3: The final shape of composite layers; (a) UHMWPE/epoxy, (b) Kevlar/epoxy, and (c) carbon/epoxy.



Figure 4: Water jet cutter.



Figure 5: The final shape of aluminum honeycomb after cutting.

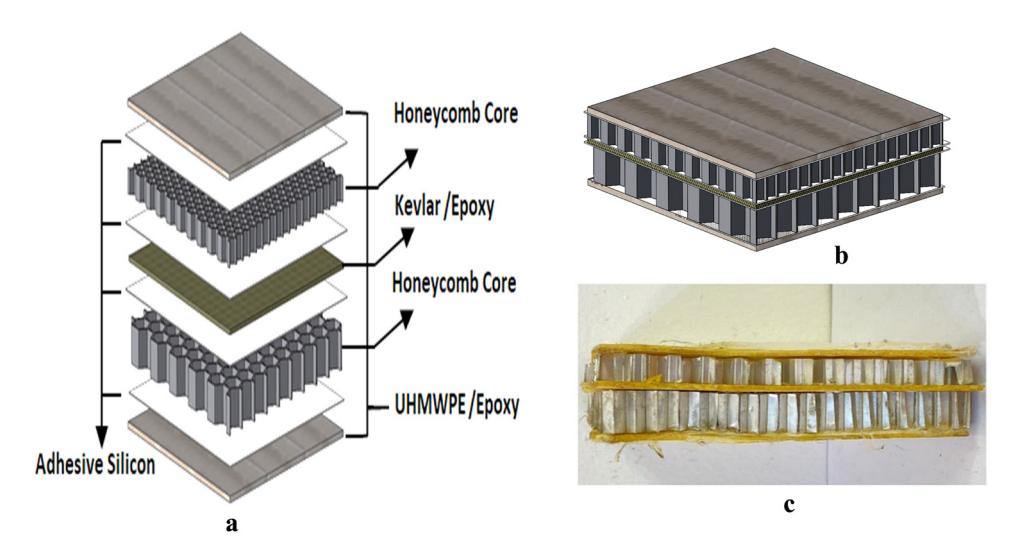


Figure 6: Hybrid sandwich body armor of first sample S1 after assembly and fabrication. (a) Schematic of arrangement of layers, (b) schematic of isometric view, and (c) photograph of side view.

machine uses computer-aided manufacturing and design systems [17].

2.4 Layers assembly and fabrication of hybrid sandwich body armor

After completing the composite layers, the layers of hybrid sandwich composite structure body armor to be fabricated were prepared. The honeycomb core was assembled (glued) with the front and back sheets using the modified-silane hybrid polymer silicon. It remained until the full silicon curing of sandwich structure body armor samples. After completing the adhesion process, the sample was left for 24 h at room temperature before using the sample in a ballistic test [18,19]. The MS hybrid polymer adhesive is excellent [20]. Figures 6–8 describe the hybrid sandwich composite body armor after assembly and fabrication for the first, second, and third samples. The three samples of hybrid sandwich body armor (150 mm × 150 mm) were made. The first sample, S1, consists of UHMWPE/epoxy, unfilled honeycomb core

(6.4 mm cell size), Kevlar/epoxy, unfilled honeycomb core (12.7 mm cell size), Kevlar/epoxy (EPX), and UHMWPE/epoxy, the second sample, S2, comprises Kevlar/epoxy, unfilled honeycomb core (6.4 mm cell size), Kevlar/epoxy, unfilled honeycomb core (12.7 mm cell size), and UHMWPE/epoxy, and the third sample, S3, comprises Al₂O₃, Kevlar/epoxy, unfilled honeycomb core (6.4 mm cell size), carbon/epoxy, unfilled honeycomb core (6.4 mm cell size), and carbon/epoxy. Table 1 provides the measurements and details of the hybrid sandwich body armor's various parts.

2.5 Ballistic test: chronograph apparatus and test procedures

The chronograph refers to an apparatus used to measure the speed of a projectile that is launched from any weapon or can be defined as a shooting speed tester. Consequently, this apparatus is one of the substantial tools used to characterize and assess any panel subject to the ballistic test [21]. Figure 9(a) manifests the beta model chronograph

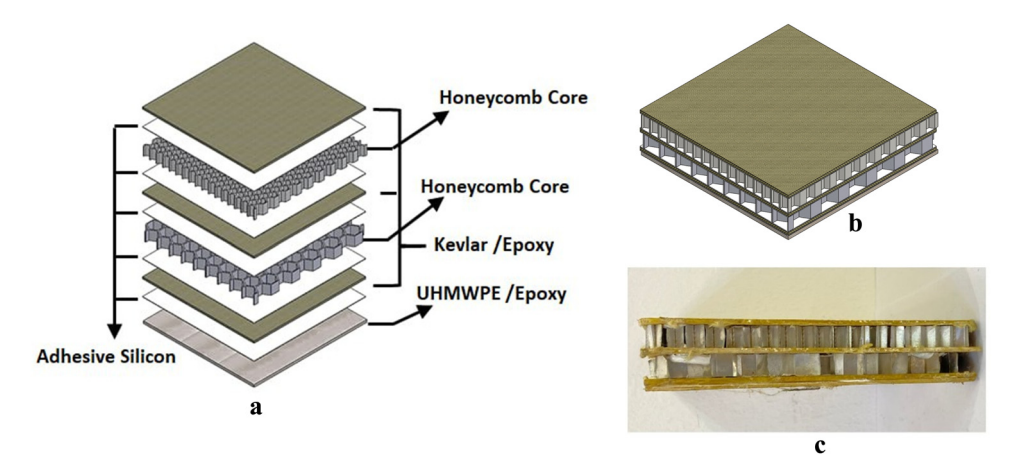


Figure 7: Hybrid sandwich body armor of second sample S2 after assembly and fabrication. (a) Schematic of arrangement of layers, (b) schematic of isometric view, and (c) photograph of side view.

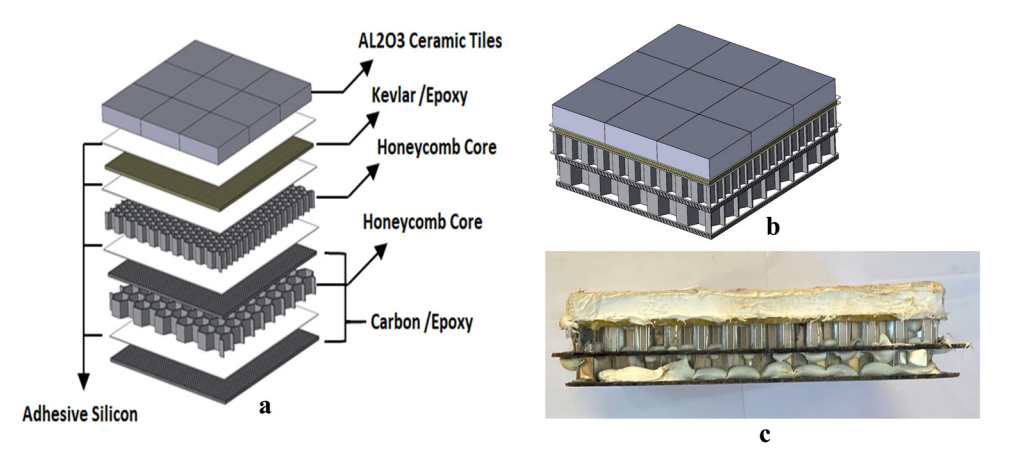


Figure 8: Hybrid sandwich body armor of third sample S3 after assembly and fabrication. (a) Schematic of arrangement of layers, (b) schematic of isometric view, and (c) photograph of side view.

used in this investigation. However, before implementing the ballistic test, the armor panel must be clamped using the backing material fixture. This equipment comprises several parts, such as a square frame, rigid plates, a hollow shaft, and the ground base [22]. Figure 9(b) reveals the equipment for the ballistic test.

To obtain a suitable ballistic response for an armor panel, it is necessary to acquire reliable data about the

Table 1: Details of the hybrid sandwich body armor components of three samples

Number of samples	Face skin material	Core material	Back skin material	Thickness (mm)		Core	Armor	Armor	Notes	
				Face skin	Core	Back skin	cell size (mm)	weight (g)	thickness (mm)	
1	UHMWPE	Aluminum honeycomb	UHMWPE	10 2 2	10 15	2	6.4 6.4	1,380	30.8	Double core with intermediate Kevlar 2 mm
2	Kevlar	Aluminum honeycomb	Kevlar UHMWPE	10 2 2	10 10	2	6.4 12.7	1,331	28.9	Double core with intermediate Kevlar 2 mm
3	Al ₂ O ₃ Kevlar	Aluminum honeycomb	Carbon	10 2 2	10 10	2	6.4 12.7		37.5	Double core with intermediate carbon 2 mm

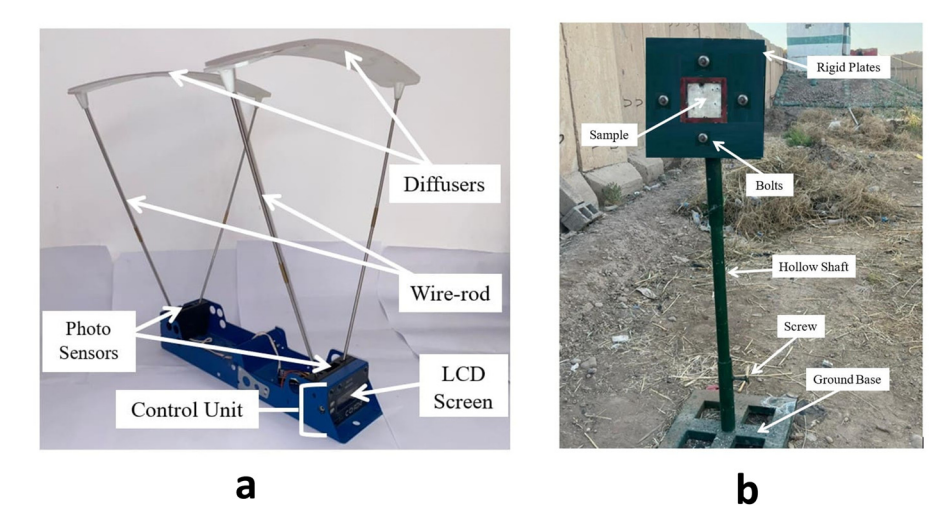


Figure 9: Schematics of (a) the chronograph device and (b) the backing material fixture.

shots. Consequently, according to the NIJ ballistic standard, a particular number of shots are required for each round of tests [23]. In effect, the complete and partial penetrations are the only two types of penetrations for any impact test. Undoubtedly, the benefit from complete penetration is to calculate the energy absorption by the armor panel, and experimentally that occurs when two devices of speed measurement are placed between the tested panels to measure the bullet speed before and after penetration. The initial or strike velocity and the residual velocity represent the velocities of the bullet before and after penetration, respectively. Hence, these velocities were used to calculate the lost energy of the bullet [24].

Set up the distance between the muzzle and the backing material fixture; this distance equals (5.0 m \pm 1.0 m). Set up the distance between the chronograph and the backing material fixture; this distance equals (2.5 m \pm 25 mm). Figure 10 shows the equipment of the ballistic test, and the whole equipment has been set up according to the standard of NIJ.

2.6 Details of projectile

The bullet 7.62×39 mm is the projectile adopted in all tests of the study. This type of caliber is so familiar in this

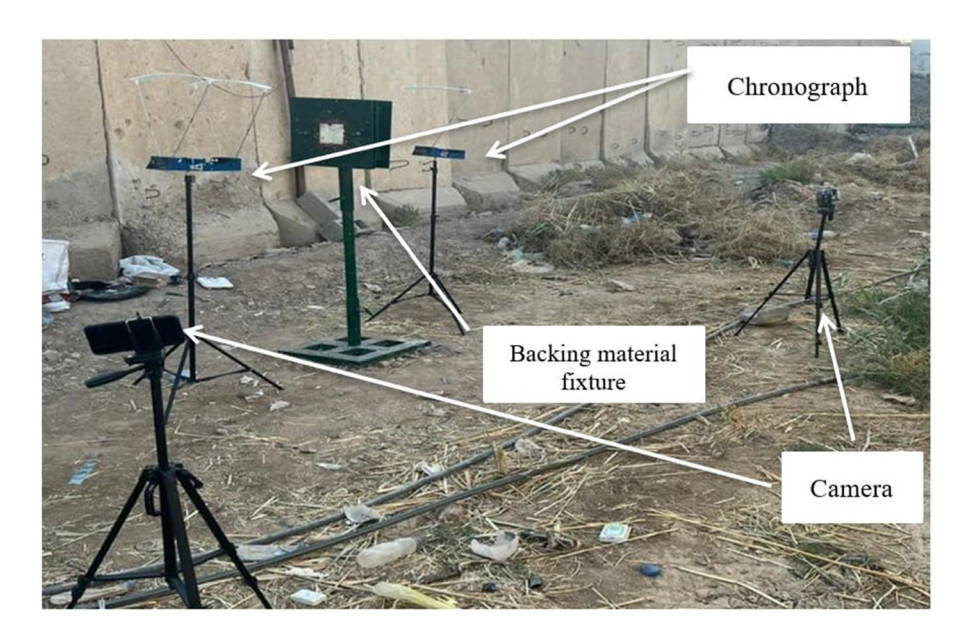


Figure 10: Photographs of the ballistic test equipment used in this study.

Table 2: Specifications of 7.62 × 39 mm bullet

Caliber	Cartridge weight (g)	Bullet weight (g)	Bullet length (mm)	Bullet diameter (mm)	Cartridge length (mm)
7.62 × 39 mm	18	8	17.3	7.62	56

domain, and many handguns shoot this ammo. All specifications of the bullet are listed in Table 2.

penetrator employed in the finite element study is displayed in Figure 11.

3 Numerical work

It is recommended to use the software LS-DYNA, ABAQUS, and ANSYS (AUTODYN) to simulate the impact of armor; this software represents the most useful and reliable tools, according to most of the cited articles [25]. This study used the commercial program ABAQUS to use the finite element approach on the hybrid sandwich composite armor. The armor model for the analysis was developed in a step-bystep manner. In the part module, geometric pieces were first constructed, after which the material properties were assigned to the parts. These components were put together in the assembly module after the creation of boundary conditions, interactions, steps, mesh, and ballistic loading with a velocity of 804 m/s. The goals of this research were then accomplished by varying the model parameters using various design matrices. Below is a discussion of the key steps in the finite element analysis.

3.1 Bullet

The bullet has a hemispherical top and a cylindrical base. This refers to a typical ballistic with a diameter of 7.62 mm and a length of 17.3 mm. It has a steel property given to it, resulting in an overall mass of 8 g [26]. The

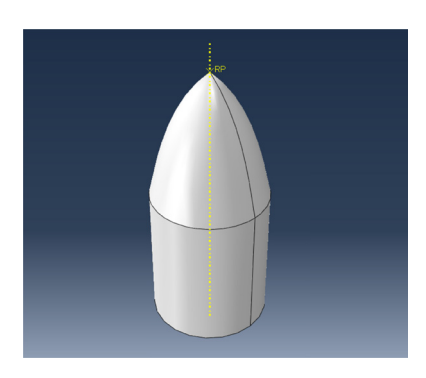


Figure 11: Steel bullet.

3.2 Armor skin layer

Kevlar and epoxy, UHMWPE and epoxy, and carbon and epoxy composites were used to design the armor's top and bottom layers. The composites were built as a 3D deformable shell 150 mm by 150 mm rectangular laminates. It was extruded to a thickness of 2 mm to evaluate the performance of the armor. These laminates have four plies, each of which is 0.5 mm thick. In weaved orientation, the plies are piled. The layers of the armor composites made of Kevlar and epoxy, UHMWPE and epoxy, and carbon and epoxy are manifested in Figure 12.

3.3 Armor honeycomb core

A honeycomb structure built of the aluminum alloy Al3003 makes up the core. A 3D deformable solid with dimensions of 150×150 mm and heights of 10 and 15 mm was used in its construction. The cells have a thickness of 0.1 mm and a size of 6.4 and 12.7 mm. The software ABAQUS depicts the honeycomb core structure in Figure 13.

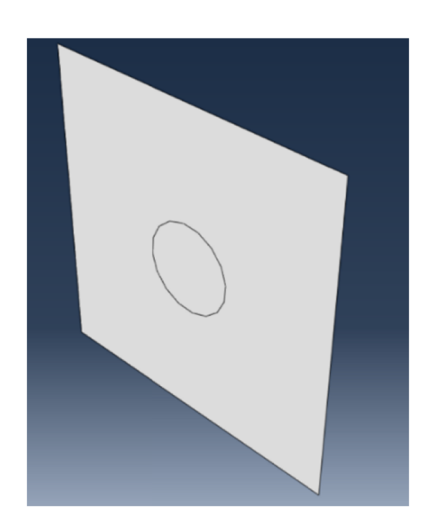


Figure 12: Armor skin layer of composites.

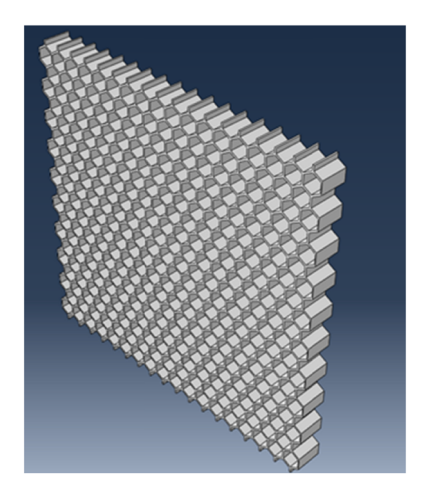


Figure 13: Aluminum honeycomb core.

3.4 Armor ceramic tiles

The tile is a ceramic structure made of Al_2O_3 , the first top layer of the armor. It was built with a 3D deformable solid with dimensions of 150 × 150 mm and a height of 10 mm. The number of tiles is nine. The software ABAQUS portrays the ceramic tiles structure in Figure 14.

3.5 Armor assembly

The geometric components are all put together, as illustrated in Figure 15. To enable the initiation of the steel bullet, a 1 mm gap was designated between the projectile and the top skin.

3.6 Armor meshing

The assembly meshing is shown in Figure 16; the total number of elements and nodes of the assembly mesh are 203,513 and 330,463, respectively.

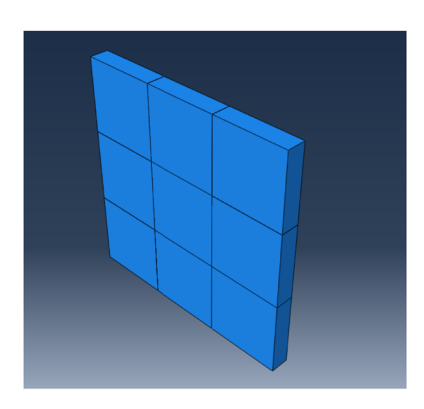


Figure 14: Al₂O₃ ceramic tiles.

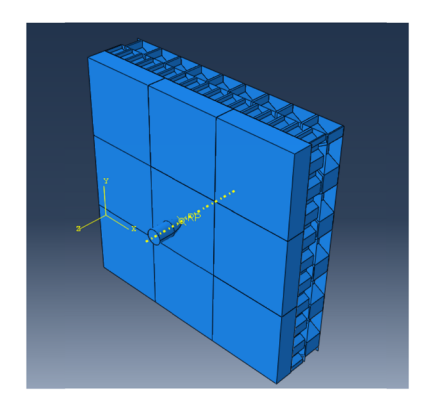


Figure 15: Armor assembly.

3.7 Armor step, interaction, and load

The final body armor model was built with 150 mm × 150 mm dimensions. The ABAQUS software widely depends on the steps in working; indeed, after constructing and assembling the geometries, generating the appropriate meshes of the model, selecting the appropriate mathematical model for materials that play a vital role in the accuracy of results, and inserting the properties of materials, the next step is how to utilize these steps to obtain a more realistic simulation. Hence, the use of these steps is different from one model to another, so the software consists of many categories, and these categories can be divided into the following main groups:

- Step: Include defining the time to conduct the simulation where the step time is 0.005 s.
- Interaction: Includes the contact between the layers and the contact between the armor and the bullet where the coefficient of friction is 0.3.
- Load: Include the boundaries, initial conditions, clamped, and the applied loads where the bullet's velocity is 840 m/s.
 Figure 17 Shows the armor clamping.

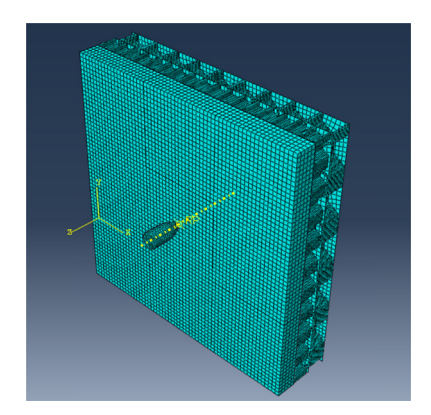


Figure 16: Assembly meshing.

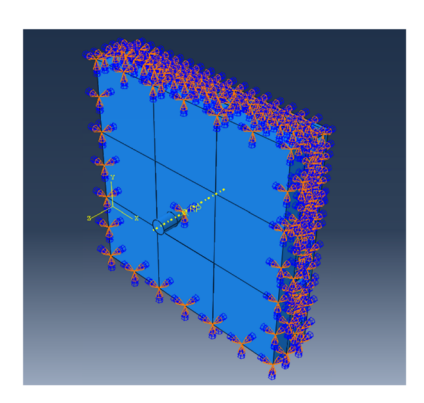


Figure 17: Armor clamping.

3.8 Armor material properties

The material properties of all geometric components that make up the armor have material properties defined. All fundamental properties of Kevlar/epoxy [27], UHMWPE/epoxy [28], carbon/epoxy [29], Aluminum alloy (AL3003) [15,30] and ceramics Al₂O₃ [16], and AISI 4140 steel alloy [31] were used in the model. Table 3 lists the mechanical properties of the bullet (AISI 4140 steel alloy).

3.9 Mesh and mesh convergence

Meshing is a crucial step required to build a model simulation for ABAQUS, so getting the appropriate meshing is required to give accurate results through several attempts to divide the total area of each part into an ideal number of elements. The output results may differ slightly depending on the mesh size selection. The number of element-level calculations may grow, as may the computing cost, but the accuracy of the results may increase with a finer mesh. It is a well-known fact that mesh refining improves the outcomes of most simulations. Prior to doing finite element analysis on the built-in hybrid sandwich armor models in this research, a mesh convergence check was performed. The goal is to produce correct findings for these models' finite element analysis. This was accomplished by employing the hybrid sandwich armor to plot the VR against the mesh sizes of

0.4, 0.6, 0.8, and 1.0 mm. The outcome confirmed the convergence, which indicated a difference of about 3% between the 0.8 and 1 mm mesh. In this investigation, a fine mesh of 0.6 mm was chosen in the hybrid sandwich structure armors' center and a coarse mesh of 3 mm at the edges. Because of the complexity of these structures, different mesh sizes were chosen. The skins' fine and coarse meshes were combined to cut down on computing time.

3.10 Materials constitutive models

The significant enhancement of computer technology and numerical analyses affected the beneficial utilization of constitutive models; indeed, selecting an appropriate constitutive model is crucial and entirely locates the insight into the actual problem and the method of analysis [32]. Hence, the study focused on understanding the constitutive material models and offered a group of essential models available in the simulation programs and used in many engineering applications. Accordingly, these models can be used as a guide for researchers in this domain of study.

3.10.1 Drucker-Prager model

To determine whether a material has failed or suffered plastic yielding, Drucker and Prager proposed the Drucker–Prager material model in 1952, which is a pressure-dependent model. The model was developed to transact soil plastic deformation. It has been used with various cohesive geological materials, including ceramic, concrete, rock, polymers, foams, and other pressure-dependent materials [33]. In this work, it has been used for ceramic tiles (SiC and $\mathrm{Al}_2\mathrm{O}_3$).

$$\sqrt{J_2} = \lambda I_1' + \kappa, \tag{1}$$

where λ and κ are Drucker-Prager material constants, J_2 is the second invariant of the stress deviator tensor, and I_1' is the first invariant of the stress tensor, and are defined as follows:

Table 3: Results of the experimental test of the hybrid sandwich composite armor samples

Samples	Initial velocity (m/s)	VR (m/s)	Ballistic limit velocity (m/s)	Areal density (kg/m²)	Energy absorption (J)	Specific energy absorption (J/kg)	DOP (mm)	BFS (mm)
S1	804	748.5	293.5366	9.688	344.65	1580.986	27.8	_
S2	804	715.3	367.0993	13.55	539.047	1767.369	_	_
S3	804	0	804	58.84	2585.66	1952.918	_	1.5

$$I_1' = \sigma_1' + \sigma_2' + \sigma_3',$$
 (2)

$$J_2 = \frac{1}{6} [(\sigma_1' - \sigma_2')^2 + (\sigma_1' - \sigma_3')^2 + (\sigma_3' - \sigma_1')^2].$$
 (3)

 $\sigma_1', \sigma_2',$ and σ_3' are the major, intermediate, and minor principal effective stresses.

3.10.2 Johnson-Cook (JC) model

The JC has been suggested in 1983. Despite being empirical and having a simple form, it is the most common model used today. However, two factors, namely, strain rate and temperature significantly impact how most materials behave. particularly alloys and metals. According to this concept, the influence of temperature and speed of strain on flow stress are alternately independent, so it is crucial to research a wide range of deformation and temperatures before designing any structure or component. In this work, this model has been used for an aluminum honeycomb core. The model can be expressed as follows [34,35]:

$$\sigma_{v} = (A + B\overline{\varepsilon}^{p^{n}})(1 + C \ln \varepsilon^{*})(1 - T^{*^{m}}), \tag{4}$$

where A, B, C, n, and m are material coefficients for the JC equation. The expression in the first series of this equation gives strain hardening term. The second series of this equation expresses the effect of strain rate, and the third series expresses the thermal effects. ε^{-p} is the equivalent plastic strain constant. ε^* is the dimensionless strain rate. A is the material's yield stress under reference deformation conditions, B is the strain hardening constant, C is the strain rate strengthening coefficient, and T^* is the homologous temperature.

$$\varepsilon^* = \frac{\varepsilon^{-p}}{\varepsilon_0},\tag{5}$$

where ε_0 is reference strain rate.

$$T^* = \frac{T - T_{\text{room}}}{T_{\text{melt}} - T_{\text{room}}},\tag{6}$$

where T is the deformation temperature, $T_{\rm room}$ is the reference deformation temperature, and T_{melt} is the material's melting temperature.

The fracture occurs when the value of D equals one, the formula for calculating *D* is as follows:

$$D = \sum \frac{\Delta \varepsilon^{-p}}{\varepsilon^{f}},\tag{7}$$

where D is the damage parameter and $\varepsilon^{\rm f}$ is the strain at fracture.

3.10.3 Hashin failure model

In the numerical analysis of composite materials, the damage initiation and modes can be judged using Hashin damage failure criteria. This model was proposed in 1980 and is considered the most popular in this field. However, this model has four failure modes, i.e., tensile failure of fiber, compression failure of fiber, tensile failure of matrix, and compression failure of matrix [36,37]. In this work, it has been used for composite materials (Kevlar, carbon, and UHMWPE).

Fiber tension ($\hat{\sigma}_{11} \ge 0$):

$$F_{\rm f}^{\rm t} = \left(\frac{\hat{\sigma}_{11}}{X^{\rm T}}\right)^2 + \alpha \left(\frac{\hat{\tau}_{12}}{S^{\rm L}}\right)^2. \tag{8}$$

Fiber compression ($\hat{\sigma}_{11} < 0$):

$$F_{\rm f}^{\rm c} = \left(\frac{\hat{\sigma}_{11}}{X^{\rm c}}\right)^2. \tag{9}$$

Matrix tension $(\hat{\sigma}_{22} \geq 0)$.

$$F_{\rm m}^{\rm t} = \left(\frac{\hat{\sigma}_{22}}{Y^{\rm T}}\right)^2 + \left(\frac{\hat{\tau}_{12}}{S^{\rm L}}\right)^2. \tag{10}$$

Matrix compression ($\hat{\sigma}_{22} < 0$):

$$F_{\rm m}^{\rm c} = \left(\frac{\hat{\sigma}_{22}}{2S^{\rm T}}\right)^2 + \left[\left(\frac{Y^{\rm C}}{2S^{\rm T}}\right)^2 - 1\right] \frac{\hat{\sigma}_{22}}{Y^{\rm C}} + \left(\frac{\hat{\tau}_{12}}{S^{\rm L}}\right)^2,\tag{11}$$

where X^{T} denotes the tensile strength in the fiber direction. X^{C} denotes the compressive strength in the fiber direction, $Y^{\rm T}$ represents the tensile strength in the direction perpendicular to the fibers, Y^{C} represents the compressive strength in the direction perpendicular to the fibers, S^L indicates the longitudinal shear strength, and S^T indicates the transverse shear strength; and α is a coefficient that determines the contribution of the shear stress to the fiber tensile initiation criterion; and $\hat{\sigma}_{11}$, $\hat{\sigma}_{22}$, and $\hat{\tau}_{12}$ are the components of effective stress tensor, $\hat{\sigma}$ that is used to evaluate the initiation criteria is computed as follows:

$$\hat{\sigma} = M\sigma, \tag{12}$$

where σ is the nominal stress and M is the damage operator.

$$M = \begin{bmatrix} \frac{1}{(1 - d_{\rm f})} & 0 & 0\\ 0 & \frac{1}{(1 - d_{\rm m})} & 0\\ 0 & 0 & \frac{1}{(1 - d_{\rm s})} \end{bmatrix}, \tag{13}$$

where $d_{\rm f}$, $d_{\rm m}$, and $d_{\rm s}$ are internal (damage) variables that characterize fiber, matrix, and shear damage, which are derived from damage variables $d_{\rm f}^{\rm t}$, $d_{\rm f}^{\rm c}$, $d_{\rm m}^{\rm t}$, and $d_{\rm m}^{\rm c}$ corresponding to the four modes previously discussed, and expressed as follows:

$$d_{\rm f} = \begin{cases} d_{\rm f}^{\rm t} & \text{if} \quad \hat{\sigma}_{11} \ge 0, \\ d_{\rm f}^{\rm c} & \text{if} \quad \hat{\sigma}_{11} < 0, \end{cases}$$
 (14)

$$d_{\rm m} = \begin{cases} d_{\rm m}^{\rm t} & \text{if} & \hat{\sigma}_{22} \ge 0, \\ d_{\rm m}^{\rm c} & \text{if} & \hat{\sigma}_{22} < 0, \end{cases}$$
 (15)

$$d_s = 1 - (1 - d_f^t)(1 - d_f^c)(1 - d_m^t)(1 - d_m^c).$$
 (16)

4 Results and discussion

This section presents the experimental and numerical results of the ballistics tests performed on the manufactured hybrid sandwich composite armor samples, and these samples have been classified based on the protection, deformation, and order of the layers. Different materials were selected to fabricate the ballistic hybrid sandwich composite body armors, including aluminum oxide ceramic tiles (Al_2O_3) having 10 mm thickness, aluminum honeycomb (6.4 and 12.7 mm cell size) possessing 10 and 15 mm thickness, carbon/epoxy composite, UHMWPE/epoxy composite, and Kevlar/epoxy composite, and all composites were of 2 mm thickness. Six parameters were used to analyze all samples after the ballistic impact of hybrid sandwich composite armor samples by the 7.62×39 mm bullet with an average impact velocity of 804 m/s. These parameters are the ability to withstand this projectile, method of layers (sheets) order, Vr, BFS, the mode of deformation, and the energy dissipation and absorption.

Figures 18–23 demonstrate the deformation behavior of the hybrid sandwich composite body armor samples (S1, S2, and S3) in real ballistic and numerical tests. These samples include the first sample (UHMWPE/epoxy, unfilled honeycomb, Kevlar/epoxy, unfilled honeycomb, Kevlar/

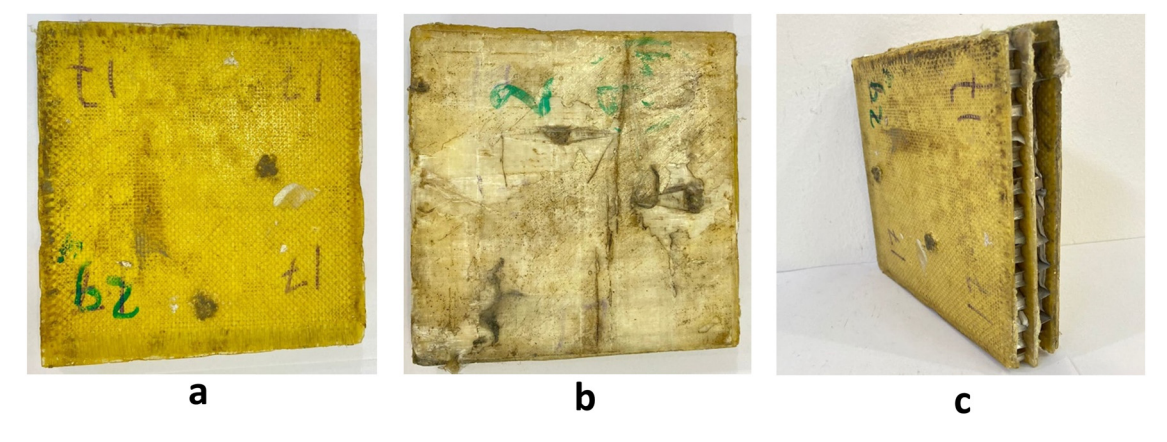


Figure 18: Photographs of the deformation of first sample (S1) after the ballistic impact (Experimental). (a) Front face, (b) back face, and (c) isometric.

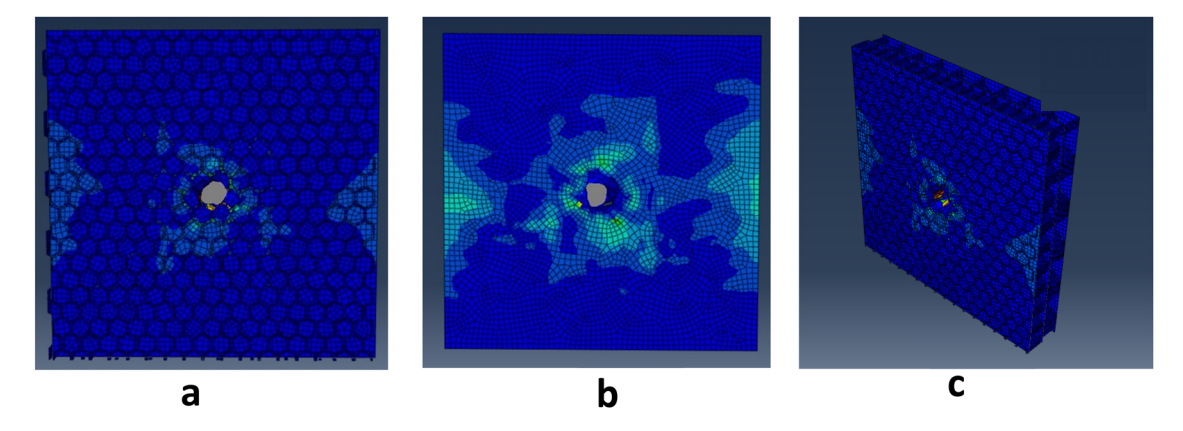


Figure 19: Photographs of the deformation of first sample (S1) after the ballistic impact (Numerical). (a) Front face, (b) back face, and (c) isometric.

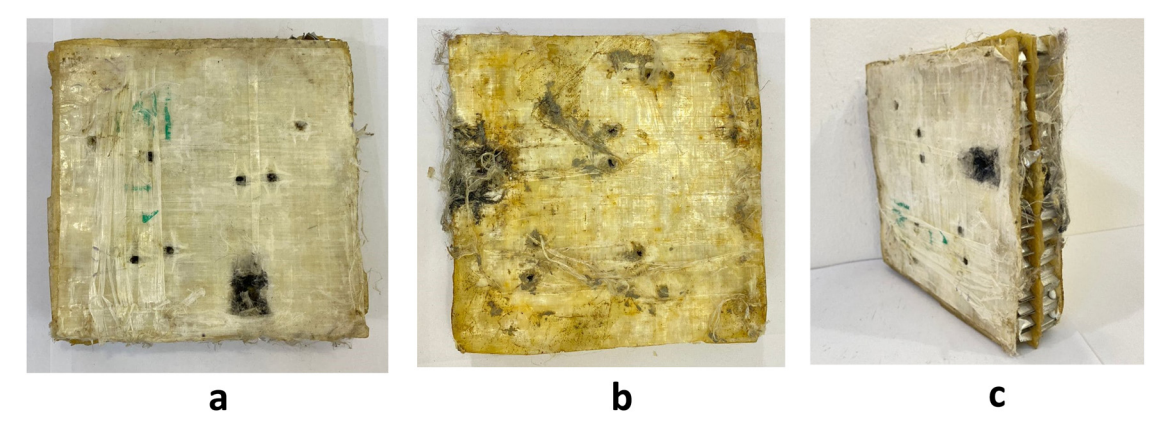


Figure 20: Photographs of the deformation of second sample (S2) after the ballistic impact (Experimental). (a) Front face, (b) back face, and (c) isometric.

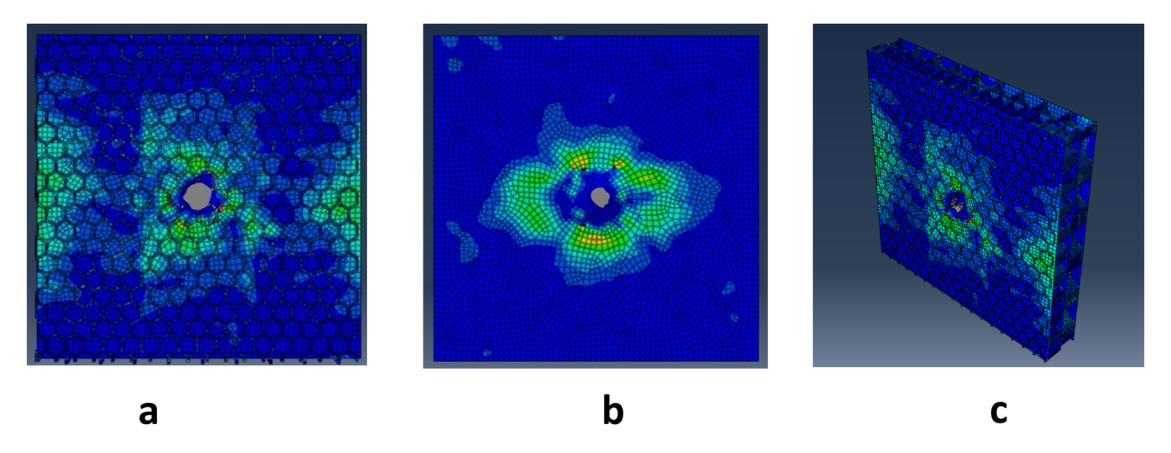


Figure 21: Photographs of the deformation of second sample (S2) after the ballistic impact (Numerical). (a) Front face, (b) back face, and (c) isometric.

EPX, and UHMWPE/epoxy), the second sample (Kevlar/epoxy, unfilled honeycomb, Kevlar/epoxy, unfilled honeycomb and UHMWPE/epoxy), and the third sample (Al_2O_3 , Kevlar/epoxy, unfilled honeycomb, carbon/epoxy, unfilled

honeycomb, and carbon/epoxy). Under the ballistic velocity impact, the hybrid sandwich composite body armors (S1 and S2) failed to stop the bullet, while the armor S3 succeeded in stopping the bullet. From these figures, it

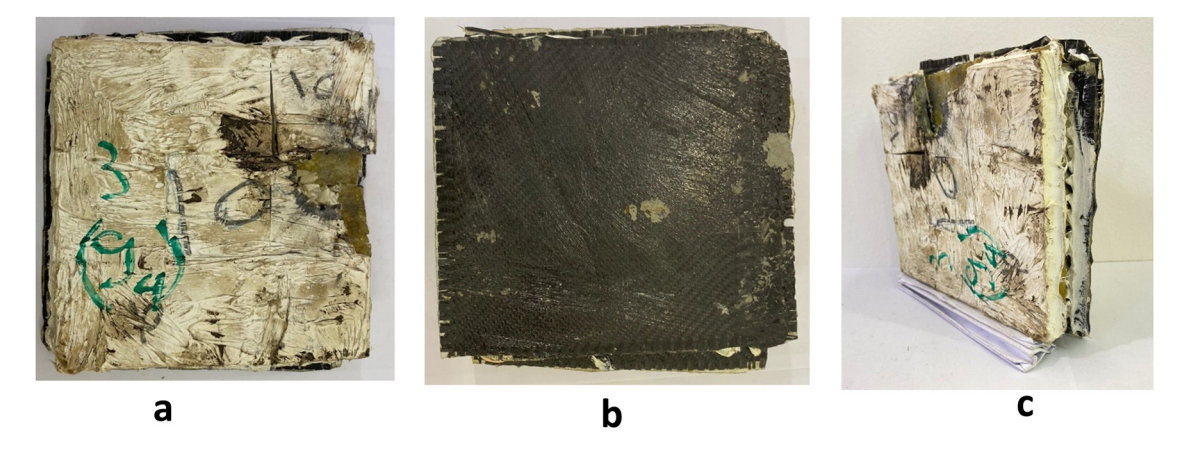


Figure 22: Photographs of the deformation of third sample (S3) after the ballistic impact (Experimental). (a) Front face, (b) back face, and (c) isometric.

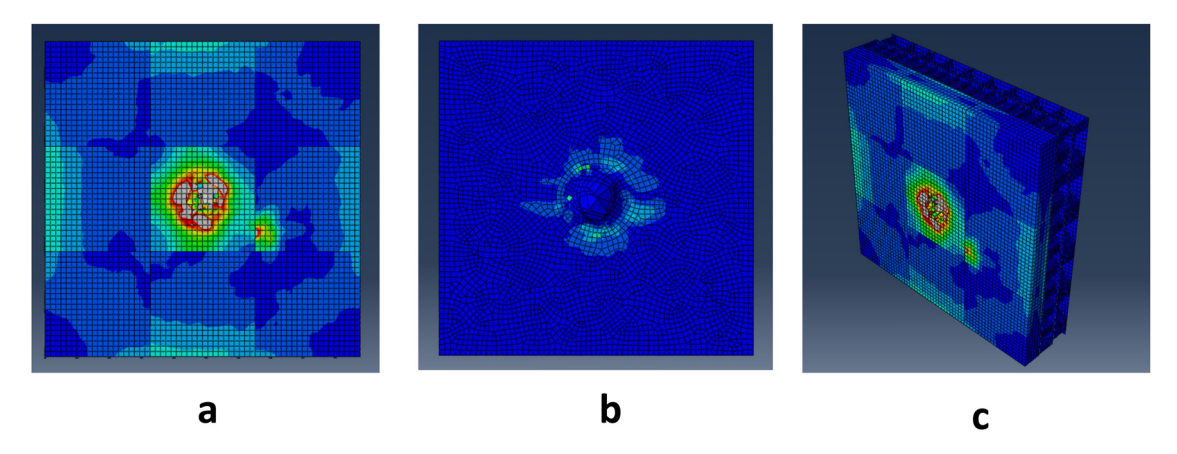


Figure 23: Photographs of the deformation of third sample (S3) after the ballistic impact (Numerical). (a) Front face, (b) back face, and (c) isometric.

can be seen that the failures of the S1 and S2 samples include the rupture of front face sheets, compression of the cells of the double honeycomb core, and rupture of the intermediate layer and back face sheet. The armors S1 and S2 failed to stop the bullet because of the absence of the ceramic tiles material in these samples, where these samples can be strengthened by adding the ceramic tiles to them to prevent penetration. The hybrid sandwich composite armor S3 system formed by the combination of the ceramic strike, Kevlar/epoxy facing sheet, double aluminum honeycomb core, carbon/epoxy intermediate layer, and carbon/ epoxy backing sheet exhibited superior ballistic performance against the Type III threat, completely stopping the projectile. This is attributed to the geometry of doubled honeycomb cores, where the compressibility of double honeycomb cores preserves the ceramic faceplates from excessive damage, and the structure of the cores helps crush and accumulate the cells under the projectile. The speeds of the

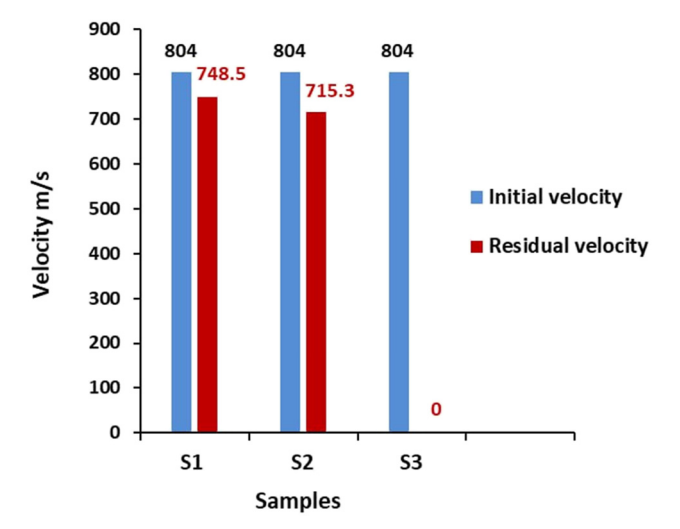


Figure 24: Initial and VR after the impact of the samples.

bullet after penetration (VR) were 748.5, 715.3, and 0 m/s, respectively. The BFS for S3 was (1.5) mm, which is optimum and within the allowed range [38]. The DOP through this armor S3 was 27.8 mm. Figure 24 illustrates the initial and VR after the impact for these samples.

The brittle crack in Kevlar/epoxy, carbon/epoxy, and UHMWPE/epoxy composites layers with perforation in (S1, S2, and S3) at the failure includes delamination, matrix spalling and pullout, and breaking and shearing failure of fibers in the layers of the composite, while in S3, the bullet can shatter the ceramic. The aluminum honeycomb's deformation appeared ductile with a large plastic deformation after the ballistic impact [39]. In S3, upon impact, the hard ceramic face plate shatters while deforming and eroding the tip of the projectile [40], where the projectile can cause ceramic failure in a ring, radial cracks form, and the resulting damage pattern in the ceramic is conical in shape and serves to spread out the impact area; however, just one tile in the impact zone was damaged. The projectile may destroy the whole ceramic plate, while smaller tiles will only receive localized damage that only has an impact on the nearby tiles, so that it is able to survive multiple impacts; benefits of using numerous tiles over a single ceramic faceplate is to limit the spread of damage, and being more durable [41]. If the ceramic is utilized with no support layers, under heavy impact force, it will break quickly due to extreme little toughness. The ceramic layer cracked and fractured, absorbing the majority of the kinetic energy of the projectile [40]. The face sheets contain a more significant number of layers than the back sheet, making the front sheets and aluminum honeycomb core absorb the projectile's remaining kinetic energy through plastic deformation and damage, supporting the damaged ceramic layer [42]. The back sheet was responsible for withstanding the compression of the front and intermediate layers and honeycomb cores and catching the fragments. The ceramics are brittle on the surface that faces the projectile, where the reduced localized pressure on the backing plate is the primary goal of the ceramic's capability to warp and degrade the projectile. Little projectile fragments stay inside the Kevlar/Epoxy and honeycomb core layers, or no fragments of this projectile could be found after the ballistics tests of armors, which suggests a complete disintegration of the 7.62 × 39 bullet. The kinetic energy of the bullet represents the magnitude of the energy which the structure of armor should absorb. Therefore, the kinetic energy undergoes a severe descent after the impact, so the speed of the bullet after penetrating the armor is inversely proportional to the amount of absorbed energy. The initial or strike velocity and the residual velocity represent the velocities of the bullet before and after penetration, respectively. Hence, these velocities have been used to calculate the absorbed energy via the following equation [43,44].

$$\Delta E = \frac{1}{2}m(v_{\rm i}^2 - v_{\rm r}^2). \tag{17}$$

 v_i , v_r , and m represent the initial and residual velocities and the mass of the bullet, respectively, as well as ΔE is the energy absorption by the sample after the ballistic impact. After calculating the initial and VR beyond the impact of the hybrid sandwich composite armors samples (S1, S2, and S3), the values of energy absorbed and specific energy absorbed were calculated. Therefore, the total energy absorption of these armors is (344.65, 539.04, and 2585.66 J) for S1, S2, and S3, respectively. Furthermore, the specific energy absorption of these armors is (1580.98, 1767.36, and 1952.91 J/kg) for S1, S2, and S3, respectively, where the specific energy absorption is the energy absorption per unit mass. Figures 25 and 26 evince the energy absorption and specific energy absorption for each sample, respectively. To provide a consistent way of comparing the

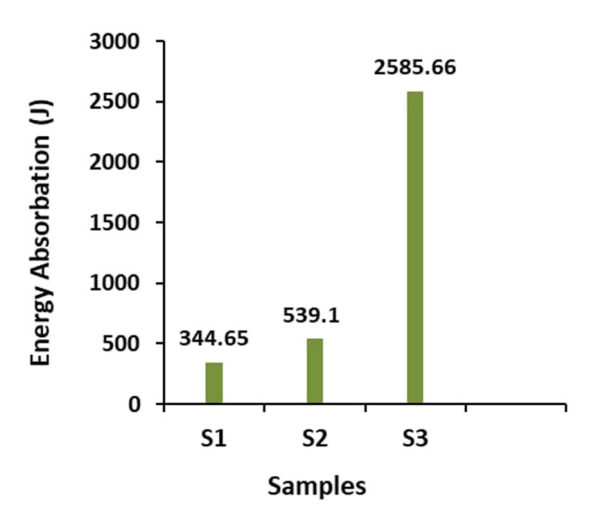


Figure 25: Energy absorption by each sample.

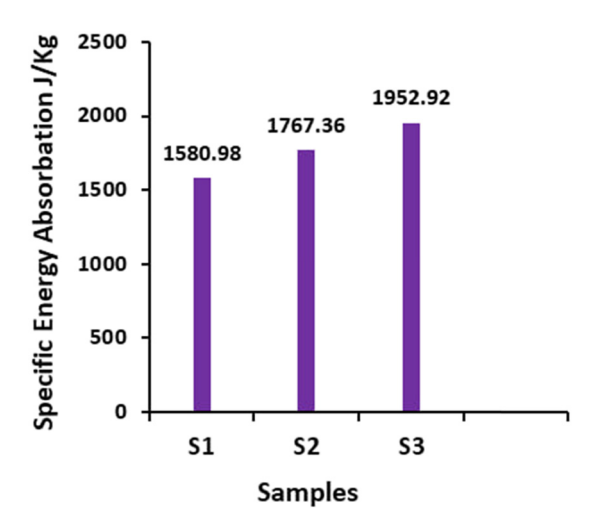


Figure 26: Specific energy absorption by each sample.

weights of armor, the term areal density was used. This is defined as the mass of armor per unit surface area and is usually stated in kg/m². The areal density of these armor samples (S1, S2 and S3) were (9.68, 13.55 and 58.84) kg/m², respectively. The ballistic limit velocity of the bullet represents the magnitude of the velocity required for a particular bullet to penetrate a particular piece of material reliably (at least 50% of the time). In other words, a given bullet will generally not pierce a given target when the bullet velocity is lower than the ballistic limit, and when the VR is zero, the ballistic limit velocity is equal to the initial impact velocity [45]. The initial and residual velocities were used to calculate the ballistic limit velocity of the bullet via the following equation [46]:

$$v_{\rm b} = \sqrt{v_{\rm i}^2 - v_{\rm r}^2}$$
, (18)

where v_b represents the ballistic limit velocity. The ballistic limit velocities of these armors were 293.53, 367.09, and 804 m/s, respectively. Figure 27 plots the ballistic limit velocity as a function of the areal density of the hybrid

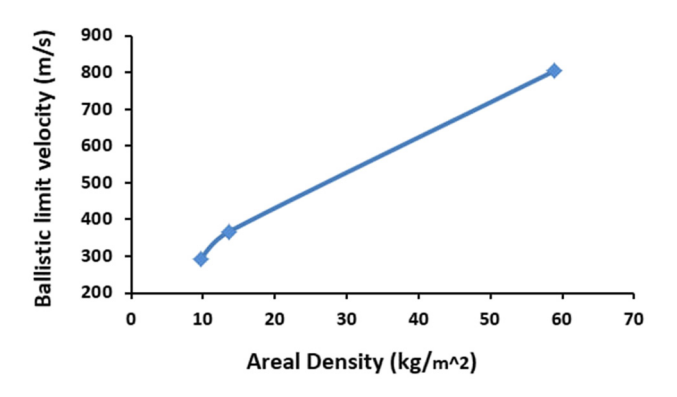


Figure 27: The ballistic limit velocity-areal density behavior of all samples.

sandwich composite armor samples. The results of this figure show that the complete penetration of S1 and S2 can be attributed to the low areal density of the armor and the early failure of each layer. The results also revealed that using the ceramic tiles in the face sheet in S3 results in a moderate percentage increase and improved ballistic limit velocity. However, this increase in ballistic limit velocity is accompanied by an increase in sample areal density. These results indicate that the ceramic tiles' ballistic resistance of the samples can be significantly enhanced, with a moderate increase in their areal density. The relation between the specific energy absorption and the areal density of the hybrid sandwich composite armor samples is shown in Figure 28. From this figure, the results demonstrate that adding ceramic tiles to the S3 face sheet improves the specific energy absorption by a significant percentage. However, the sample areal density increase coincides with this increase in specific energy absorption. These results manifest that, with a moderate increase in areal density, the sample's ability to absorb energy can be significantly improved by employing ceramic tiles. Table 3 lists the resulting values of the ballistic test of initial velocity, VR, ballistic velocity, areal density, energy absorption, specific energy absorption, DOP, and BFS of the hybrid sandwich composite armor samples experimentally. Table 4 depicts the resulting values of the ballistic test of initial velocity, VR,

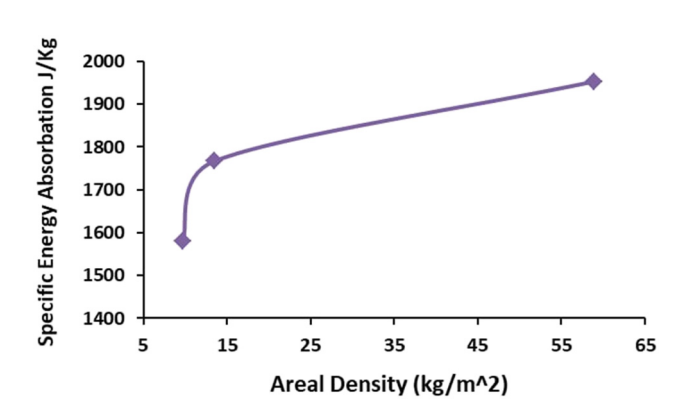


Figure 28: The specific energy absorption-areal density behavior for all samples.

Table 4: Results of the numerical test of the hybrid sandwich composite armor samples

Samples	Initial velocity (m/s)	VR (m/s)	BFS (mm)
S1	804	755	_
S2	804	719	_
S3	804	0	1.7

Table 5: Results deviation of the VR

Sample	VR (m	Deviation %		
	Experimental	Numerical		
S1	748.5	756.8	1.10	
S2	715.3	729.9	2.04	

and BFS of the hybrid sandwich composite armor samples numerically.

The validation of numerical simulations is essential, especially in modeling the protective structures, due to the high rate of the kinetic energy of this event. In general, to validate the BFS of modeling, the following relation was used to calculate the deviation of the numerical results to the exact values recorded in the ballistic test:

Deviation%
$$= \frac{\text{(Experimental results - Numerical results)}}{\text{Experimental results}}.$$
 (19)

After using this equation to calculate the deviation of numerical results, the results elucidated a good agreement between the experimental and numerical results of the BFS. Table 5 shows the deviation of VR results. If the comparison is made among the S1, S2, and S3, S3 is the best and strongest, and it was able to stop the bullet due to the presence of ceramic tiles and the structure of the cores, which helps compress and accumulate the cells under the projectile. In the double core, the compressing and accumulating of the cells is increased, whereas it cushions the bullet and begins to compress and densify in a localized region.

5 Conclusion

In this work, hybrid composite sandwich structures were manufactured and tested experimentally and numerically. After analyzing the experimental results of the work, this work presents the fundamental conclusion and highlights the essential results that contributed to the evaluation of the hybrid sandwich armors performance. However, the ballistic impact of using a 7.62×39 mm bullet offered crucial points that explain the importance of this structure. The analysis of the ballistic behavior of the S3 armor elucidated the ability of this armor to absorb all the energy of impact except S1 and S2, which were penetrated by the bullet. The BFS of the S3 armor was 1.5 mm, which is optimum and within the allowed range. The DOP through

the armor S3 was 27.8 mm. Also, the energy absorption according to the velocity of the initial impact of the S1, S2, and S3 were 344.65, 539.04, and 2585.66 J, respectively. Furthermore, the ballistic limit velocity of these armors was 293.53, 367.09, and 804 m/s, respectively. On comparing the samples S1, S2, and S3, S3 was found to be the best and strongest, and it was able to stop the bullet due to the structure of cores, which helps compress and accumulate the cells under the projectile, as it cushions the bullet and begins to compress and densify in a localized region.

The results of the experimental and numerical work comparison elucidated a good agreement between these approaches, with a significant matching in the failure pattern. The deviation of the VR result of numerical modeling from the experimental work is acceptable and limited between 1.10 and 2.04% for S1 and S2, respectively. Finally, the software of ABAQUS is one of the most reliable software; hence, this study highly recommends using this software in the ballistic field, and it also recommends evaluating the performance of this armors under ballistic impacts by using the last type of ammunitions 30 caliber M2 AP after the pre-last type used in this study is 7.62×39 mm bullet.

6 Recommendations and future works

The number of observations might serve as a reflection of a particular insight, and these points of view serve as a crucial road map for enhancing this unique form of body armors; therefore, several recommendations can be made for future work in this field of study, some of these recommendations are:

- · Create new hybrid sandwich composite structure designs of body armors via a selection of new hybrid sandwich systems.
- Change the core's geometry to another geometry, such as an auxetic, corrugated, and chiral shape.
- Evaluate the performance of these armors under ballistic impacts by using ammunition such as a 30 caliber M2 AP (IV level).
- Use new ballistic materials for the core, front and back sheets of these designs of body armors.
- · Change the thickness and cell size of the core and the thickness of the front and back sheets.
- Use advanced materials such as nanotubes, nanomaterials, or natural fibers in the armor's structures.
- It is recommended to use functionally graded materials in the armor's structures.

Funding information: Authors declare that this manuscript was done depending on the personal effort of the author, and there is no funding effort from any side or organization.

Conflict of interest: The authors state no conflict of interest with anyone related to the subject of the manuscript or any competing interest.

Data availability statement: Most datasets generated and analyzed in this study are comprised in this submitted manuscript. The other datasets are available on reasonable request from the corresponding author with the attached information.

References

- [1] Abtew MA, Boussu F, Bruniaux P. Dynamic impact protective body armour: A comprehensive appraisal on panel engineering design and its prospective materials. Def Technol. 2021;17(6):2027-49.
- Council NR. Opportunities in protection materials science and [2] technology for future army applications. Washington, DC: National Academies Press; 2011.
- Thomas EL. Opportunities in protection materials science and technology for future Army applications. Adv Ceram Armor VIII.
- Kumar KN, Kumar CB, Kumar KH, Noolvi B. Investigation of composite sandwich plates for ballistic armor application. Mater Today: Proc. 2020;27:1738-42.
- Ramanathan A, Krishnan PK, Muraliraja R. A review on the production of metal matrix composites through stir casting-Furnace design, properties, challenges, and research opportunities. J Manuf Process. 2019:42:213-45.
- Medvedovski E. Ballistic performance of armour ceramics: [6] Influence of design and structure. Part 1. Ceram Int. 2010;36(7):2103-15.
- Stanisławek S, Morka A, Niezgoda T. Pyramidal ceramic armor [7] ability to defeat projectile threat by changing its trajectory. Bull Pol Acad Sci: Tech Sci. 2015;(4):843-9.
- Liu MP, Zhu D, Yao Y, Wang J, Bui TQ. Numerical simulation of ballistic impact behavior of bio-inspired scale-like protection system. Mater Des. 2016;99:201-10.
- [9] Mullaoğlu F, Usta F, Türkmen HS, Kazancı Z, Balkan D, Akay E. Deformation behavior of the polycarbonate plates subjected to impact loading. Procedia Eng. 2016;167:143-50.
- Hu D, Zhang Y, Shen Z, Cai Q. Investigation on the ballistic behavior of mosaic SiC/UHMWPE composite armor systems. Ceram Int. 2017;43(13):10368-76.
- de Oliveira Braga F, Da Luz FS, Monteiro SN, Lima Jr ÉP. Effect of the [11] impact geometry in the ballistic trauma absorption of a ceramic multilayered armor system. J Mater Res Technol. 2018;7(4):554-60.
- Liu X, Li M, Li X, Deng X, Zhang X, Yan Y, et al. Ballistic performance of UHMWPE fabrics/EAMS hybrid panel. J Mater Sci. 2018;53:7357-71.

- [13] Yang J-S, Chen S-Y, Li S, Pang Y-Z, Schmidt R, Schröder K-U, et al. Dynamic responses of hybrid lightweight composite sandwich panels with aluminium pyramidal truss cores. J Sandw Struct & Mater. 2021;23(6):2176–95.
- [14] Hassoon OH, Abed MS, Oleiwi JK, Tarfaoui M. Experimental and numerical investigation of drop weight impact of aramid and UHMWPE reinforced epoxy. J Mech Behav Mater. 2022;31(1):71–82.
- [15] Tan Y, Wang X, Ma M, Zhang J, Liu W, Fu R, et al. A study on microstructure and mechanical properties of AA3003 aluminum alloy joints by underwater friction stir welding. Mater Charact. 2017:127:41–52.
- [16] Jiang J-F, Wu Y-F. Identification of material parameters for Drucker–Prager plasticity model for FRP confined circular concrete columns. Int | Solids Struct. 2012;49(3–4):445–56.
- [17] Rao DB, Baskey D, Rawat R, editors. Water jet cutter: an efficient tool for composite product development. Proceedings of the national conference on scientific achievements of SC & ST Scientists & Technologists. U.K.: Connecting Repositories; 2009.
- [18] Al-Khazraji MS, Bakhy SH, Jweeg MJ. Modal analysis of specific composite sandwich structures. Eng Technol J. 2023;41(1):13–22.
- [19] Saleem IA, Abed MS, Ahmed PS. Numerical and experimental study of hybrid composite body armor. Eng Technol J. 2021;39(11):1681–7.
- [20] Mosa MH, Hamzah MN. Evaluating the adhesive properties of four types of conventional adhesives. Eng Technol J. 2022;40(1):120–8.
- [21] Rule WK, Jones S. A revised form for the Johnson-Cook strength model. Int | Impact Eng. 1998;21(8):609-24.
- [22] Mosa MH, Hamza MN, editors. Influence of selection materials and construction techniques on the ballistic performance of armors: A review. AIP Conference Proceedings. AIP Publishing; 2021.
- [23] Shin Y-H, Chung J-H, Kim J-H. Test and estimation of ballistic armor performance for recent naval ship structural materials. Int J Nav Archit Ocean Eng. 2018;10(6):762–81.
- [24] PROGRAMS DOJWDOOJ. Ballistic resistance of body armor. NIJ Standard-0101.06: 2008.
- [25] Mosa MH, Hamza MN, editors. Evaluating the performance of a unique design of biomimetic armor. AIP Conference Proceedings. AIP Publishing; 2022.
- [26] Khalaf WA, Hamzah MN. Numerical investigation of impact resistance of honeycomb composite armor. MESM Modeling Conference. Eurosis-Eti Publishing; 2022.
- [27] Lim H, Hoag SW. Plasticizer effects on physical–mechanical properties of solvent cast Soluplus® films. Aaps Pharmscitech. 2013;14:903–10.
- [28] Han L, Cai H, Chen X, Zheng C, Guo W. Study of UHMWPE fiber surface modification and the properties of UHMWPE/epoxy composite. Polymers. 2020;12(3):521.
- [29] Varelidis P, McCullough R, Papaspyrides C. The effect on the mechanical properties of carbon/epoxy composites of polyamide coatings on the fibers. Compos Sci Technol. 1999;59(12):1813–23.

- [30] Ferrasse S, Hartwig KT, Goforth RE, Segal VM. Microstructure and properties of copper and aluminum alloy 3003 heavily worked by equal channel angular extrusion. Metall Mater Trans A. 1997;28:1047–57.
- [31] Lapczyk I, Hurtado JA. Progressive damage modeling in fiberreinforced materials. Compos Part A: Appl Sci Manuf. 2007;38(11):2333–41.
- [32] Herle I. Fundamentals of constitutive modelling for soils. ALERT Doctoral School. 2021; Constitutive Modelling in Geomaterials. 3.
- [33] Alejano LR, Bobet A. Drucker-prager criterion. The ISRM suggested methods for rock characterization, testing and monitoring: 2007–2014. Cham: Springer International Publishing; 2014. p. 247–52.
- [34] Lin YC, Chen XM, Liu G. A modified Johnson–Cook model for tensile behaviors of typical high-strength alloy steel. Materials Science and Engineering. 2010;52726:6980–6.
- [35] Kıranlı E. Determination of material constitutive equation of a biomedical grade Ti6AI4V alloy for cross-wedge rolling. Doctoral dissertation. Turkey: Izmir Institute of Technology; 2009.
- [36] Hashin Z, Rotem A. A fatigue failure criterion for fiber reinforced materials. J Composite Mater. 1973;7(4):448–64.
- [37] Hashin Z. Fatigue failure criteria for unidirectional fiber composite. J Appl Mech. 1980;47(4):329–34.
- [38] Enforcement NL, Center CT. Selection and application guide to personal body armor. US Department of Justice, Office of Justice Programs. Washington, DC: National Institute of Justice; 2001.
- [39] Nieoczym A, Drozd K. Fractographic assessment and FEM energy analysis of the penetrability of a 6061-T aluminum ballistic panel by a fragment simulating projectile. Adv Sci Technol Res J. 2021;15(1):50-7.
- [40] Naik N, Kumar S, Ratnaveer D, Joshi M, Akella K. An energy-based model for ballistic impact analysis of ceramic-composite armors. Int | Damage Mech. 2013;22(2):145–87.
- [41] Florence AL Interaction of projectiles and composite armor, Part II. Report AMMRCCR-69-15Stanford Research Institute, Menlo Park; 1969.
- [42] Medvedovski E. Lightweight ceramic composite armour system. Adv Appl Ceram. 2006;105(5):241–5.
- [43] Sikarwar RS, Velmurugan R, Madhu V. Experimental and analytical study of high velocity impact on Kevlar/Epoxy composite plates. Cent Eur J Eng. 2012;2:638–49.
- [44] Arora S, Ghosh A. Evolution of soft body armor. Adv Text Eng Mater. 2018;7:499–552.
- [45] Ben-Dor G, Dubinsky A, Elperin T. Analytical engineering models of high speed normal impact by hard projectiles on metal shields. Open Eng. 2013;3(3):349–73.
- [46] Recht R, Ipson TW. Ballistic perforation dynamics. J Appl Mech. 1963;30(3):384–90.